CO Adsorption on Noble Metal Clusters: Local Environment Effects

ARTICLE *in* THE JOURNAL OF PHYSICAL CHEMISTRY C · MARCH 2011

Impact Factor: 4.77 · DOI: 10.1021/jp108763f

3 AUTHORS, INCLUDING:

Daniel E Resasco
University of Oklahoma
331 PUBLICATIONS **10,988** CITATIONS

SEE PROFILE

THE JOURNAL OF PHYSICAL CHEMISTRY C

ARTICLE

pubs.acs.org/JPCC

CO Adsorption on Noble Metal Clusters: Local Environment Effects

Brian H. Morrow, Daniel E. Resasco, and Alberto Striolo*

School of Chemical, Biological and Materials Engineering, The University of Oklahoma, Norman, Oklahoma 73019, United States

Marco Buongiorno Nardelli

Department of Physics, North Carolina State University, Raleigh, North Carolina 27695, United States, and Computer Science and Mathematics Division, Oak Ridge National Laboratory, Oak Ridge, Tennessee 37831, United States

ABSTRACT: We have used ab initio density functional theory calculations to study the adsorption of CO on clusters of 13 noble metal atoms. The cluster composition ranges from 100% Pt to 100% Au. Because our goal is to study the effect of local environment on CO adsorption, adsorption is only studied on the top atom site. This atom can be either Pt or Au, depending on the cluster considered. Results are analyzed in terms of CO adsorption energy, CO bond stretching frequency, geometry of the CO + cluster system, and HOMO−LUMO gaps. It is found that, as expected, the CO adsorption energy on Pt is >1 eV more favorable than that on Au and that the cluster composition affects both adsorption energy and stretching frequency. Specifically, when CO adsorbs on Pt, increasing Au content decreases the adsorption energy. In contrast, when CO adsorbs on Au, increasing Pt content increases the adsorption energy. In general, higher adsorption energies lead to lower C−O stretching frequencies. Electronic-structure details (i.e., density of states) are discussed to explain the observed results, toward improving the interpretation of experimental spectroscopic data and possibly designing new catalysts.

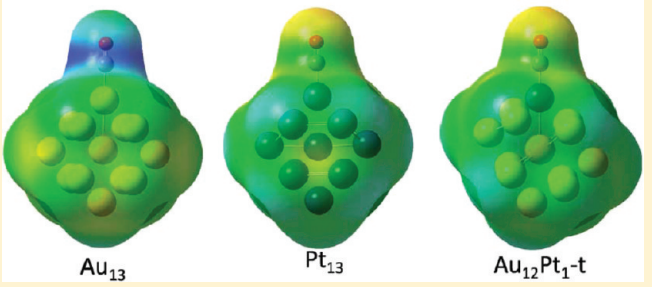

INTRODUCTION

Bimetallic catalysts are useful because of their versatility, such as the ability to tune their catalytic activity and selectivity by varying properties such as composition, particle size, and support.[1] In particular, Pt−Au catalysts have been shown to exhibit enhanced activity and selectivity in specific reactions when compared to monometallic catalysts. For example, Dimitratos et al.[2] showed that carbon-supported Pt−Au has higher catalytic activity for the oxidation of glycerol than carbon-supported Pt and that the catalyst preparation method affects the selectivity. Selvarani et al.[3] determined that the optimum Pt:Au ratio for carbon-supported Pt−Au as a direct methanol fuel cell catalyst is 2:1, at which composition the catalyst delivers a peak power density 1.5 times that of pure Pt. Comotti et al.[4] found a turnover frequency of 60 h^{-1} for the oxidation of glucose over pure platinum, while a Pt−Au alloy with Au:Pt ratio of 2:1 yields a turnover frequency of 924 h^{-1}. The authors also found that, for 7 different Au:Pt ratios ranging from 4 to 0.25, the minimum and maximum turnover frequencies are 240 and 924 h^{-1}, observed for Au:Pt ratios of 1 and 2, respectively. It is likely that these results depend on the atomic arrangement on the surface of the bimetallic nanoparticles used as catalysts. Unfortunately, direct experimental visualization of the composition and structure of nanoparticle surfaces is at present problematic, especially at operating conditions. Techniques such as high-energy resonant X-ray diffraction can be used to probe the structure of bimetallic catalysts.[5] Molecular simulations could be useful to interpret such experiments and also identify the local structure of supported mono- and bimetallic nanoparticles.[6−8] For example, we have previously used molecular dynamics (MD) simulations to study the effect of composition and support geometry on the properties of Pt−Au nanoparticles containing 250 atoms,[9] finding that it should be possible to tailor the distribution of atoms by manipulating nanoparticle composition and support geometry. This could lead to greater control of catalyst selectivity by maximizing the active sites on the nanoparticle surface that catalyze a certain reaction.

In order to link our previous MD results to experimentally verifiable measurements, we report here ab initio density functional theory (DFT) calculations for CO adsorption on Pt−Au clusters. CO is often employed as a probe molecule because its adsorption energy and C−O stretching frequency depend on the adsorption site, as can be observed experimentally via, e.g., Fourier transform infrared spectroscopy.[10] CO adsorption is also important in CO oxidation, which occurs in automobile catalytic converters,[11] in preferential CO oxidation (PROX reaction) in hydrogen feeds,[12] and in CO hydrogenation, the critical step in Fischer−Tropsch processes.[13] DFT has been used to study adsorption of CO on metal surfaces, such as Pt(111),[14−17] on Pt(111) overlayers,[18,19] and on metal nanoparticles.[20] For example, Sadek and Wang[21] have investigated CO adsorption on Pt/Au clusters containing two to four atoms,

Received: September 14, 2010
Revised: January 24, 2011
Published: March 07, 2011

while Song et al.[22] have reported adsorption energies for CO on Pt/Au clusters of up to seven atoms. Sadek and Wang[21] found that CO vibrational frequency and CO bond length depend primarily on the adsorption site. Specifically, bridge site adsorption leads to CO bond vibrational frequencies in the range 1737−1927 cm^{-1} and bond lengths in the range 1.167−1.204 Å, irrespective of cluster composition. When adsorption occurs on the top site, vibrational frequencies are in the range 2000−2091 cm^{-1} and bond lengths are in the range 1.151−1.167 Å. These results did not show a direct relationship between adsorption energy and CO bond vibrational frequency, although the authors found that CO frequency decreases linearly with the decrease in CO bond length. Song et al.[22] found that CO adsorption on Pt atoms is more favorable than that on Au atoms. They found that cluster composition affects the adsorption energy, and in particular they found that when CO adsorbs on Au atoms the most favorable cluster composition is that with 25% Pt. They also found that, for a six-atom cluster, CO adsorption energy increases with Pt composition. They did not report data for either CO bond stretching frequency or CO bond length. A detailed understanding of how the cluster composition affects the observed results remains elusive.

Pedersen et al.[23] have performed experiments involving Pt overlayers on Au(111). Among their findings was the fact that CO adsorption was weaker on single Pt atoms in the Au(111) surface than on pure Pt(111) surfaces. They also found that a monolayer of Pt on Au(111) exhibits stronger CO adsorption than pure Pt(111). Nilekar et al.[19] showed via DFT calculations that CO adsorption on Pt(111) overlayers on Ru is much weaker than on pure Pt(111) surfaces and also that the monolayer coverage on the former material is much less than on the latter. Combining DFT results with experiments, they demonstrated that these effects lead to potent catalysts for the PROX reaction, even when conducted at mild conditions.[18] Habrioux et al.[24] found an increase in CO−Pt binding energy with increasing gold content in nanoparticles with diameters of ∼4−10 nm. Irissou et al.[25] synthesized Pt−Au films that also showed an increase in CO adsorption energy with increasing Au content. These experimental findings, in agreement with DFT calculations conducted on flat surfaces, appear to disagree with the DFT results of Song et al.[22] discussed above, which were obtained for metal clusters of <10 atoms. This discrepancy suggests that size effects can play a very important role in the properties of metal nanoparticles and clusters. For example, Pt clusters containing 8−10 atoms have been shown to have a 40−100 times greater activity for the oxidative dehydrogenation of propane than a Pt-coated monolith.[26] This brief literature survey suggests the need of better understanding the catalytic properties of metal clusters of various sizes.

In this manuscript we investigate CO adsorption on Pt and Au atoms in Pt−Au clusters of 13 atoms. Our goal is to quantify how the local environment around the metal atom on which adsorption occurs affects the properties of the adsorbed CO. We study how the CO adsorption energy, C−O stretching frequency, and cluster morphology depend on the cluster composition. All our calculations are conducted using Pt−Au clusters containing 13 atoms. This cluster size allows us to have a central atom surrounded by an outer shell while maintaining the total number of atoms low enough to maintain the computational cost tractable. Thirteen-atom Pt clusters have been studied previously because they form closed-shell cubooctahedral and icosahedral structures.[27] While smaller than nanoparticles used in most industrial and academic applications of catalysis, including those considered in our MD simulations,[9,28−30] these clusters could serve as a useful model for atoms with low coordination numbers, such as those on corners and edges of nanoparticles, which are expected to have high catalytic activity. Because, as discussed above, particle size appears to play an important role in CO adsorption in bimetallic clusters and nanoparticles, DFT calculations covering a wide range of particle sizes could help elucidate this size effect. Such calculations are beyond the scope of this manuscript. We found that C−O stretching frequency and CO adsorption energy are inversely related, with higher adsorption energies leading to lower C−O stretching frequencies. To explain the local environmental effects on the properties of adsorbed CO, we studied the electronic properties of the clusters, calculating the charges of relevant atoms, the energy differences between highest occupied and lowest unoccupied molecular orbitals (HOMO−LUMO gaps), and the density of states for the various clusters.

The remainder of this paper is organized as follows. First we describe the details of our calculations. Next we discuss results for cluster geometries, CO adsorption energy, and C−O stretching frequency. We then explain the observed trends in adsorption energy and frequency.

COMPUTATIONAL DETAILS

Ab initio density functional theory (DFT) calculations were performed using Gaussian03.[31] We performed calculations using six different exchange-correlation functionals: (1) the Becke three-parameter hybrid functional[32] with the nonlocal correlation functional of Lee, Yang, and Parr[33] and the local correlation functional of Vosko, Wilk, and Nusair[34] (B3LYP);[35] (2) the functional of (1) but with the nonlocal correlation functional of Perdew[36] (B3P86); (3) Becke's 1988 exchange functional[37] with Perdew and Wang's 1991 gradient-corrected correlation functional[38,39] (BPW91); (4) the exchange and correlation of Perdew and Wang's 1991 functional (PW91); (5) the functional of Perdew, Burke, and Ernzerhof[40] (PBE); and (6) the PBE functional as rendered into a hybrid by Adamo[41] (known as PBE0, but referred to as PBE1PBE in Gaussian). Quantitative comparisons between the results are given as an Appendix to the text. All the results reported in the main text were obtained using the B3LYP functional, which was chosen because of its agreement with experimental results and its previous use in similar calculations.[17,42−45]

The LANL2DZ effective core potential and basis set[46] was used to describe metal atoms, while the 6-311G* basis set was used to describe C and O atoms. Calculations for an isolated CO molecule match the experimental bond length of 1.13 Å.[47] The calculated C−O stretching frequency of 2212 cm^{-1} overestimates the experimental value of 2143 cm^{-1} by ∼3%.

Clusters containing 13 metal atoms were used in our calculations. We studied both Au_{13} and Pt_{13}. We generated other clusters by replacing one atom in Au_{13} (Pt_{13}) with Pt (Au). When the replaced atom is in the center of the cluster, the cluster name is designated by "-c". The atom on which CO is adsorbed is referred to as the "top" atom. When that atom is replaced, the cluster is designated as "-t". By this naming convention, the clusters studied here are designated as Au_{13}, $Au_{12}Pt_1$-c, $Pt_{12}Au_1$-t, $Au_{12}Pt_1$-t, $Au_{12}Pt_1$-c, and Pt_{13} (see Figure 1). In our calculations Pt_{13}, $Au_{12}Pt_1$-t, and $Au_{12}Pt_1$-c had spin multiplicities of 3, while $Pt_{12}Au_1$-c, $Pt_{12}Au_1$-t, and Au_{13} had spin multiplicities of 2. No spin−orbit coupling effects were considered in our calculations.

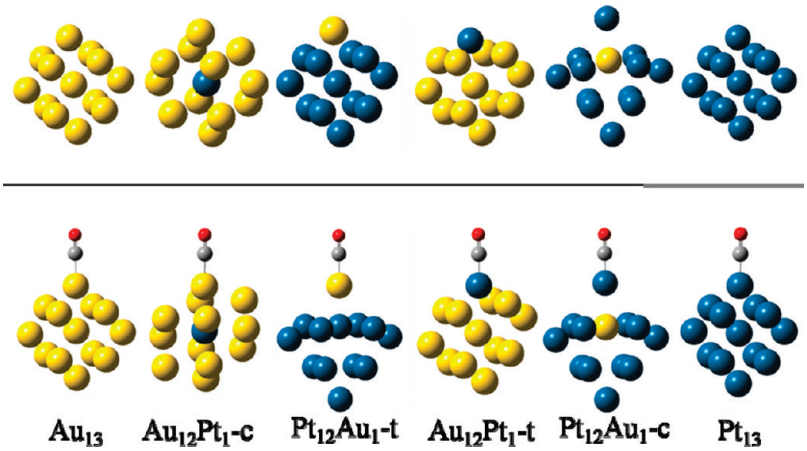

Figure 1. Top: optimized geometries of 13-atom metal clusters. Bottom: optimized geometries of 13-atom clusters with adsorbed CO. Pt, Au, C, and O atoms are represented by blue, yellow, gray, and red spheres, respectively.

Adsorption energies are calculated by subtracting the sum of the energies of isolated CO and the metal cluster from the energy of the metal cluster with adsorbed CO. More negative values indicate stronger adsorption. Density of states calculations were performed using the program GaussSum 2.2.[48] Atomic charges were calculated by the natural bond orbital analysis (NBO), using the NBO version 3 program contained in Gaussian.[49,50]

RESULTS AND DISCUSSION

a. Cluster Geometry. Optimized geometries of the six clusters studied with and without adsorbed CO, with no symmetry restraints, are shown in Figure 1. In three of the clusters (Au_{13}, $Au_{12}Pt_1$-c, and $Pt_{12}Au_1$-t), CO is adsorbed on Au, and in the other three ($Au_{12}Pt_1$-t, $Pt_{12}Au_1$-c, and Pt_{13}), CO is adsorbed on Pt. Our previous MD simulations, conducted at 700 K for Pt−Au bimetallic nanoparticles of 250 atoms,[9] indicated, in agreement with a number of theoretical[51−54] and experimental[55−58] results, that Au tends to segregate to the outer shell of Pt−Au bimetallic nanoparticles. However, individual Pt atoms can still be found at the surface of such bimetallic nanoparticles.[59,60] It should also be pointed out that experimental techniques are available to prepare Pt adlayers on gold, even though such structures are not stable at high temperatures.[18]

In some of the energy-minimized structures for the 13-atom clusters in Figure 1 (e.g., in the $Pt_{12}Au_1$-c cluster), Au is located in the cluster interior. It should be noted that DFT calculations are effectively conducted at 0 K and that the energy minimization procedure does not guarantee that the global minimum energy structure of the clusters has been reached. Rather, the energy minimization routine finds a local minimum on the potential energy surfaces. In fact, $Pt_{12}Au_1$-t is 2.46 eV more stable than $Pt_{12}Au_1$-c prior to CO adsorption. With CO adsorbed, the energy difference decreases to 1.3 eV. Prior to adsorption, $Au_{12}Pt_1$-c is 1.15 eV more stable than $Au_{12}Pt_1$-t. Upon CO adsorption, the complex CO+$Au_{12}Pt_1$-t is more stable than CO+$Au_{12}Pt_1$-c by 0.25 eV, due to the strong adsorption energy of CO on Pt. This change of the energetic stability of $Au_{12}Pt_1$-t vs $Au_{12}Pt_1$-c upon CO adsorption may be related to changes in the morphology of heterogeneous catalysts under reaction conditions, a topic not further discussed here.

Table 1. Bond Lengths in CO + Cluster Systems

cluster	C−metal distance (Å)	C−O distance (Å)
Au_{13}	1.993	1.133
$Au_{12}Pt_1$-c	1.984	1.133
$Pt_{12}Au_1$-t	1.948	1.133
$Au_{12}Pt_1$-t	1.852	1.147
$Pt_{12}Au_1$-c	1.807	1.152
Pt_{13}	1.834	1.149

The energy-minimized clusters of Figure 1 are used to study the adsorption of CO and therefore assess the effect of local environment on adsorption energy and vibrational frequency, quantities that are experimentally observable. By comparing the structures of the metal clusters before and after CO adsorption (top and bottom panels in Figure 1, respectively), we observe that CO adsorption results in minimal changes in the geometries of the clusters, except in the case of $Pt_{12}Au_1$-t, which will be discussed below.

Distances between the C atom of CO and the metal atom on which it is adsorbed, as well as those between C and O atoms in adsorbed CO, are reported in Table 1. When CO is adsorbed on Au, the C−metal distance ranges from 1.948 Å, on $Pt_{12}Au_1$-t, to 1.993 Å, on Au_{13}. When CO is adsorbed on Pt, the C−metal distance is ∼0.1−0.15 Å shorter and ranges from 1.807 Å, on $Pt_{12}Au_1$-c, to 1.852 Å, on $Au_{12}Pt_1$-t. Comparing the C−metal to the C−O distance, we find, for CO adsorbed on Pt, that the shorter the C−metal distance is, the longer the C−O bond becomes. The C−O distance ranges from 1.147 Å, on $Au_{12}Pt_1$-t, to 1.152 Å, on $Pt_{12}Au_1$-c. The Pt−C distance is shortest for CO on $Pt_{12}Au_1$-c and not for CO on Pt_{13}, as might have been expected. For CO adsorbed on Au, the C−O distance is 1.133 Å for all three systems studied. Based on these results, one could speculate that adsorption on Pt changes the CO electronic structure significantly, while adsorption on Au does not perturb to a large extent the CO electronic structure.

b. Adsorption Energy. The adsorption energy for CO on the six metal clusters is reported in Figure 2. The adsorption is the weakest on Au_{13}, −0.66 eV, and it is the strongest on Pt_{13}, −2.40 eV.

Experiments for CO adsorption on alumina-supported Pt nanoparticles give an adsorption energy of −2.13 eV, in reasonable agreement with our results.[61] However, oxide supports can alter the catalytic properties of the supported metals, so it is possible that this is not a valid comparison. The CO adsorption

dx.doi.org/10.1021/jp108763f |J. Phys. Chem. C 2011, 115, 5637–5647

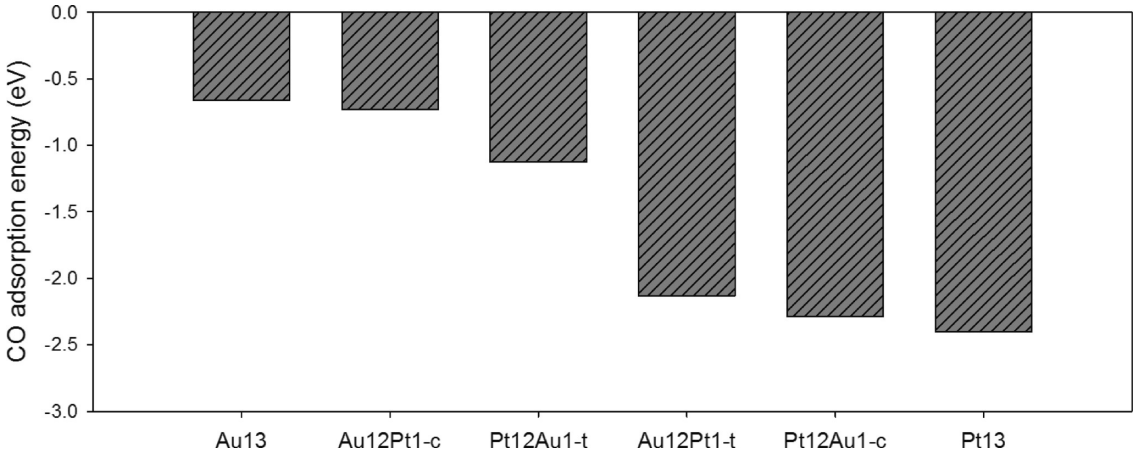

Figure 2. CO adsorption energy on 13-atom metal clusters. For identification of the clusters, see Figure 1.

energy on Pt(111) is ~1.9 eV,[62] and DFT calculations have shown that as cluster sizes decrease the CO adsorption energy increases relative to that on Pt(111),[63] in qualitative agreement with our results. Experimental CO adsorption energies on TiO_2-supported Au nanoparticles with size of 1.8−3.1 nm were found to range from 0.54 to 0.79 eV.[64] Ion bombardment of Au(111) gives low-coordinated atoms similar to those in our clusters; the CO adsorption energy was found to be −0.56 eV on such a surface.[65] Similar adsorption energies (−0.53 eV) were also found for Au nanoparticles supported by highly oriented pyrolytic graphite.[65] Additional validation could be attained by comparing our results to theoretical literature reports. Previous DFT calculations yield adsorption energies of −2.86 eV[21] for CO on Pt_4 and −2.73 eV[66] for CO on Pt_6, in reasonable agreement with our findings.

Not surprisingly, our calculations show adsorption energies >1 eV stronger (more negative) when CO adsorbs on Pt than when it adsorbs on Au.

More importantly for the scope of the present paper, however, is that the results show that changing the composition of the cluster has a quantifiable effect on the adsorption energy even when CO adsorbs on the same metal atom (i.e., Au or Pt). When CO adsorbs on Au, increasing the Pt content of the cluster increases the adsorption energy. When the central atom of Au_{13} is replaced by Pt, the adsorption energy increases (i.e., becomes more negative) by 0.07 eV; when CO adsorbs on a single Au atom in an otherwise Pt cluster ($Pt_{12}Au_1$-t), the adsorption energy is 0.40 eV higher than on Au_{13}. In contrast, when CO adsorbs on the Pt top atom, increasing the Au content within the cluster decreases the adsorption energy. When the central atom of Pt_{13} is replaced by Au, the adsorption energy becomes less negative by 0.12 eV; the adsorption energy on $Au_{12}Pt_1$-t is 0.27 eV lower than on Pt_{13}. Pedersen et al.[23] showed experimentally that the CO desorption temperature is lower on single Pt atoms in Au(111) than for clean Pt(111), analogous to our result of lower CO adsorption energy on $Au_{12}Pt_1$-t than Pt_{13}. Temperature-programmed desorption experiments by Ren et al. showed that Au/Pt binds CO more weakly than pure Pt.[67] This results in less coking and CO poisoning of the catalyst and is consistent with our DFT calculations. To highlight the relevance of our calculations, we point out that changes in the CO adsorption energy on transition metal catalysts of the order of ~0.5 eV have led to the design of effective catalysts that promote the PROX reaction at mild conditions.[18,19] We notice that, in general, as the adsorption energy increases (becomes more negative), the C−metal distance decreases and the C−O distance increases (see Table 1). Some deviations from this general trend are, however, evident from our results (compare, for example, the results obtained on Pt_{13} vs those on $Pt_{12}Au_1$-c).

c. C−O Stretching Frequency. Values for the C−O stretching frequency are reported in Figure 3. Although we could rescale our CO vibrational frequency results to account for differences from experimental values in the gas phase, we prefer to report the raw data. The experimental value[61] for CO adsorbed on alumina-supported Pt nanoparticles is 2075 cm^{-1}. Gruene et al.[68] experimentally measured single-molecule CO adsorption on group 10 transition metal clusters and reported a value of ~2070 cm^{-1} for CO on Pt_{13}. These results are comparable to our calculated value of 2091 cm^{-1} for CO on Pt_{13}, especially when we recall that our calculations overestimate the vibrational frequency for isolated CO (2212 vs 2143 cm^{-1} found experimentally). Meier and Goodman[64] found experimental frequencies of ~2123 cm^{-1} for CO adsorbed on Au nanoparticles with sizes of 1.8−3.1 nm, also in reasonable agreement with our calculations. As expected from the Blyholder model,[69] because of differences in adsorption energies, the C−O stretching frequency is larger for CO adsorbed on Au and lower for CO adsorbed on Pt.

Our results show that the local environment affects the C−O stretching frequency. In the case of CO adsorbed on Pt, increasing the Au content of the cluster slightly increases the C−O stretching frequency. Replacing the central atom of Pt_{13} with Au results in a frequency of 2093 cm^{-1}, while the frequency for CO on $Au_{12}Pt_1$-t is 2100 cm^{-1}. Frequencies for CO adsorbed on Au are ~70−80 cm^{-1} higher than those for CO on Pt.

According to the Blyholder model,[69] the C−O stretching frequency is expected to increase as the adsorption energy decreases (the decreased back-donation of electrons results in weaker adsorption, leading to a stronger C−O bond). Consequently, the vibration frequencies should be highest on Au_{13}, and progressively lower for $Au_{12}Pt_1$-c and $Pt_{12}Au_1$-t. This trend is generally obeyed by our data, as can be seen from Figure 3. Our results show the highest stretching frequency for CO on $Pt_{12}Au_1$-t.

The somewhat peculiar behavior of the $Pt_{12}Au_1$-t cluster can be explained by examining the optimized geometries shown in Figure 1. In the $Pt_{12}Au_1$-t cluster, the Au atom is pulled away from the Pt ones, leaving the former isolated at the top of the cluster. This geometrical effect changes the electronic properties of the Au atom, resulting in different CO adsorption behavior

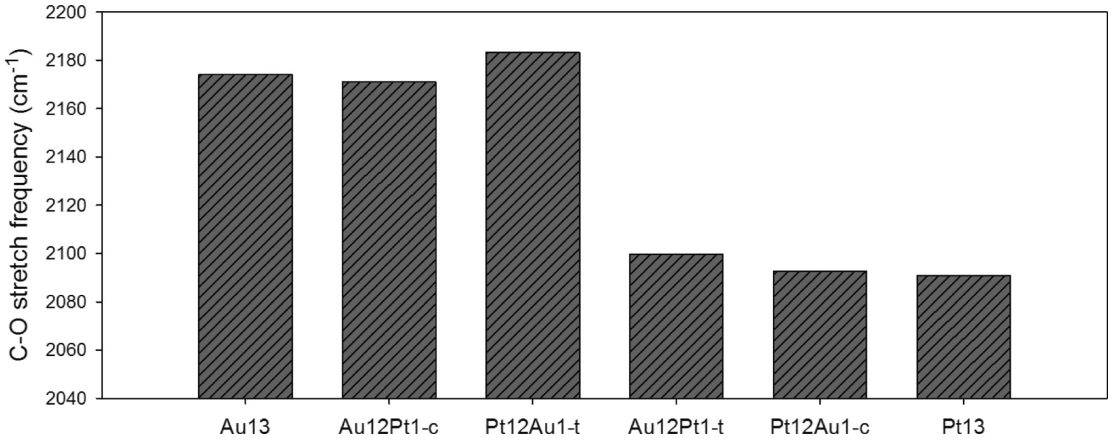

Figure 3. C−O stretching frequency for CO adsorbed on 13-atom metal clusters. For identification of the clusters, see Figure 1.

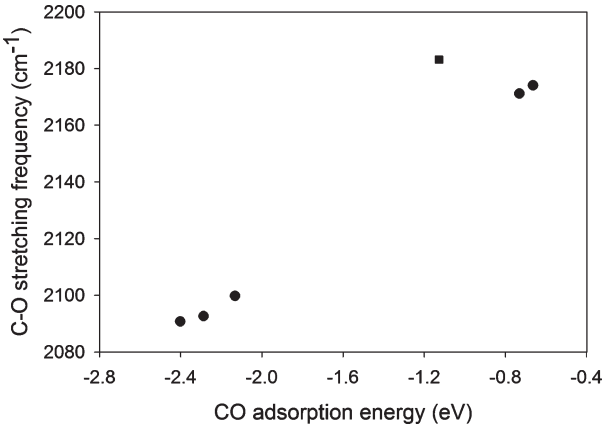

Figure 4. C−O stretching frequency vs CO adsorption energy, data from Figure 2 and Figure 3. The square represents results obtained for CO adsorption on $Pt_{12}Au_1$-t.

compared to that on the "top" Au atoms in Au_{13} and $Au_{12}Pt_1$-c. Calculations for CO adsorption on a single Au atom (not discussed in detail here for sake of brevity) support this hypothesis, yielding a C−O stretching frequency of 2180 cm^{-1}, very close to the frequency of 2183 cm^{-1} found for CO on $Pt_{12}Au_1$-t.

In Figure 4 we report the relationship between C−O stretching frequency and CO adsorption energy. The result for the high frequency observed on the $Pt_{12}Au_1$-t cluster is included as a square symbol to differentiate it from the other data points. As can be seen from Figure 4, our results show that as the CO stretching frequency decreases the adsorption energy becomes more negative. It is important to reiterate that for all cases considered in Figure 4 CO adsorbs on top of either Pt or Au and that changes in both adsorption energy and vibrational frequency are due to changes in the cluster composition (i.e., local environment). Changes in the adsorption site (e.g., adsorption between adjacent metal atoms) have not been considered.

d. Atomic Charges. To attempt rationalizing why CO adsorption energy changes for clusters of different compositions and to determine if there is a correlation between atomic charges in the clusters and the adsorption energy, we calculated the atomic charges on various atoms. There is no consensus in the literature on how to rigorously calculate atomic charges.[70] All currently available methods, which include the Mulliken population analysis,[71] the electrostatic potential (ESP),[72] and the natural bond orbital (NBO) methods,[49,50] involve approximations. We have used the NBO method, as it has been found to be in good agreement with Lewis structure concepts and give accurate results for bond hybridization and polarization.[73]

Reported in Figure 5 are the charges for carbon and oxygen atoms when CO is adsorbed on the clusters. Additionally, we report the charges of the top metal atom, both for bare clusters (no adsorbed CO) and for the clusters with adsorbed CO. In the left panel of Figure 5, the first three clusters considered on the *x*-axis have CO adsorbed on Au, while in the last three CO is adsorbed on Pt.

Comparing the charge on the carbon and oxygen atoms of CO prior to and after adsorption (left panel), it might be possible to differentiate among different mechanisms of CO adsorption on the various clusters. However, the results do not show significant changes when the cluster composition is altered. We can only report that when CO is adsorbed on Pt, the charge of the oxygen atom is slightly more negative than when CO adsorbs on Au, possibly a consequence of electronic back-donation.

For systems with CO adsorbed on Pt, the adsorption energy is reported as a function of the charge on the top metal atom prior to CO adsorption in the right panel of Figure 5. As the metal cluster composition changes, the charge in the top metal atom also changes. As the charge on the top metal atom prior to CO adsorption becomes more positive, the CO adsorption energy increases, going from −2.13 eV when the charge is −0.20*e* to −2.40 eV when the charge is 0.15*e*. This could indicate that a lower electron density on the top Pt atom results in more electron donation from the carbon atom of adsorbing CO, yielding stronger adsorption. There is no corresponding trend when adsorption occurs on Au, suggesting that the electronic phenomena leading to CO adsorption differ when CO adsorbs on Pt or on Au.

e. HOMO−LUMO Gaps. In order to characterize the electronic structure of the clusters considered, we calculated the difference in energy between the highest occupied and lowest unoccupied molecular orbitals (HOMO−LUMO gaps). From a catalytic perspective, systems with smaller HOMO−LUMO gaps tend to be more reactive.[74,75] In Table 2 we report the HOMO−LUMO gaps for the clusters studied here, both with and without adsorbed CO. The results obtained for the HOMO−LUMO gap for the metal clusters before CO adsorption are identified as "bare" clusters. For these, we find that Au_{13} and Pt_{13} have the highest and lowest HOMO−LUMO gaps, respectively. In general, correlating the results in Table 2 to data

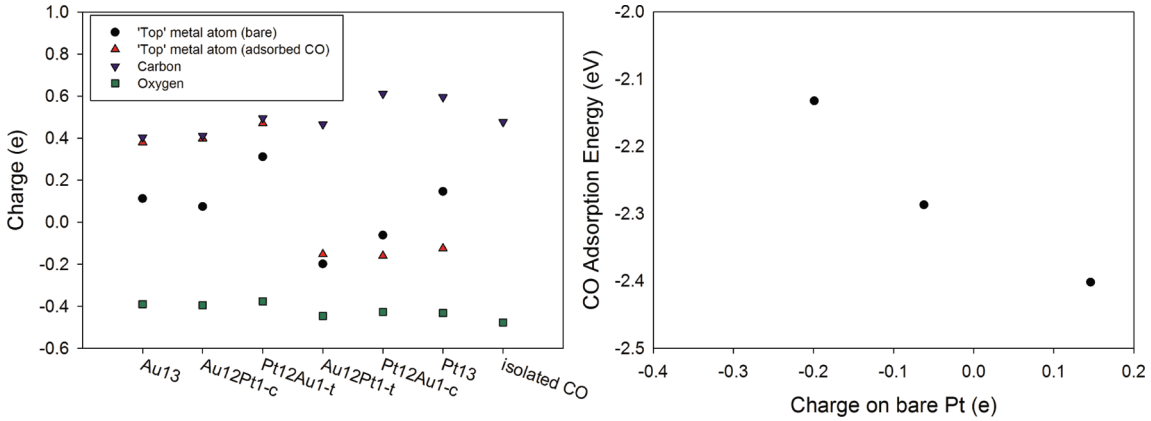

Figure 5. Left panel: charges for top metal atoms on bare metal clusters, for top metal atoms on clusters with adsorbed CO, and for C and O atoms of adsorbed CO. Right panel: CO adsorption energy as a function of charge of top Pt atoms. All charges are calculated using the natural bond orbital method.[49,50].

Table 2. HOMO−LUMO Gap Calculations for 13-Atom Clusters in Vacuum (Bare) or with Adsorbed CO

cluster	HOMO−LUMO gap, bare cluster (eV)	HOMO−LUMO gap, CO + cluster (eV)
Au_{13}	1.497	1.252
$Au_{12}Pt_1$-c	1.279	1.170
$Pt_{12}Au_1$-t	1.361	0.844
$Au_{12}Pt_1$-t	1.306	1.361
$Pt_{12}Au_1$-c	1.088	0.844
Pt_{13}	0.925	0.762

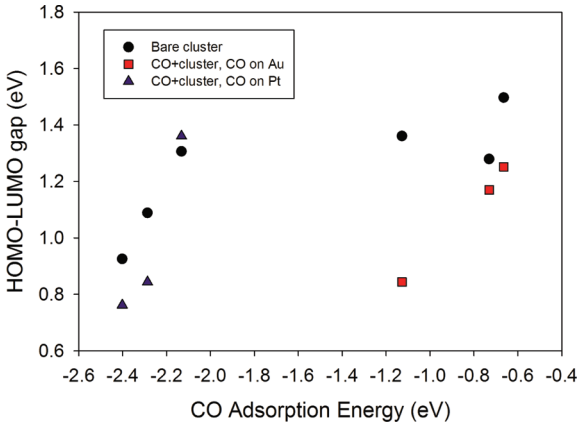

Figure 6. HOMO−LUMO gaps as a function of CO adsorption energy.

for CO adsorption energy, we observe that a lower HOMO−LUMO gap for the bare clusters results in higher CO adsorption energy (see Figure 6). However, our data suggest that the correlation just described holds only when CO adsorbs on the same type of metal (i.e., either Pt or Au). Further, because the trend just documented is not obeyed for the $Au_{12}Pt_1$-c cluster (which has the third-lowest HOMO−LUMO gap, while CO adsorption on $Au_{12}Pt_1$-c shows the second-lowest energy of the systems considered), it appears that CO adsorption on Pt is more easily explained than that on Au. For the clusters with adsorbed CO, Pt_{13} again has the lowest HOMO−LUMO gap, but $Au_{12}Pt_1$-t has the highest.

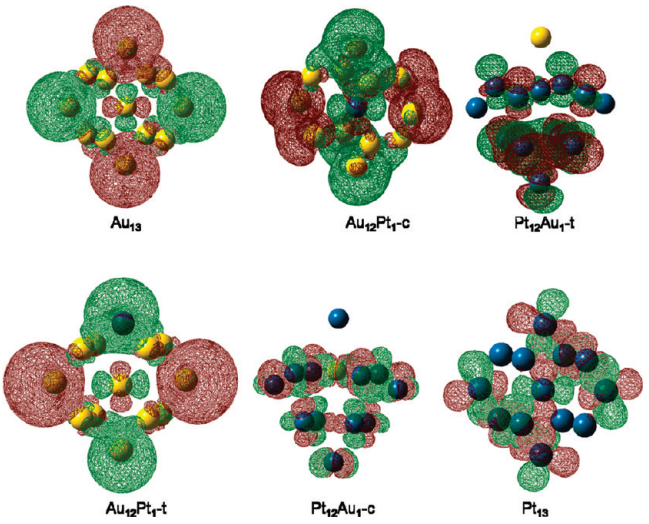

Figure 7. Highest occupied molecular orbitals (HOMOs) for bare metal clusters. Pt and Au atoms are represented by blue and yellow spheres, respectively. Red and green represent positive and negative phases, respectively.

To visualize the effect of cluster composition on the overall electronic structure, we report in Figure 7 the highest occupied molecular orbitals for the bare clusters. Visualizations of both highest occupied and lowest unoccupied molecular orbitals for each cluster considered here, with and without adsorbed CO, are not reported for brevity.

f. Density of States. In order to gain a deeper insight of the electronic mechanisms that play a role in the adsorption properties of CO, we analyzed the density of states (DOS) projected on the metal atom on which CO adsorbs, as well as on the C and O atoms of CO. Differences in densities of states can indicate changes in reactivity. It has been shown[23,76−78] that the center of the d-band relative to the Fermi energy plays a role in the reactivity of transition metals in different environments. For a variety of metals and adsorbates, it has been shown that adsorption energy increases as the d-band center shifts to higher energies. For example, Kitchin et al.[77] used DFT calculations to show that a subsurface alloy shifted the d-band center of Pt(111) and that a lower d-band center led to a decrease in dissociative adsorption energy for hydrogen and oxygen. These

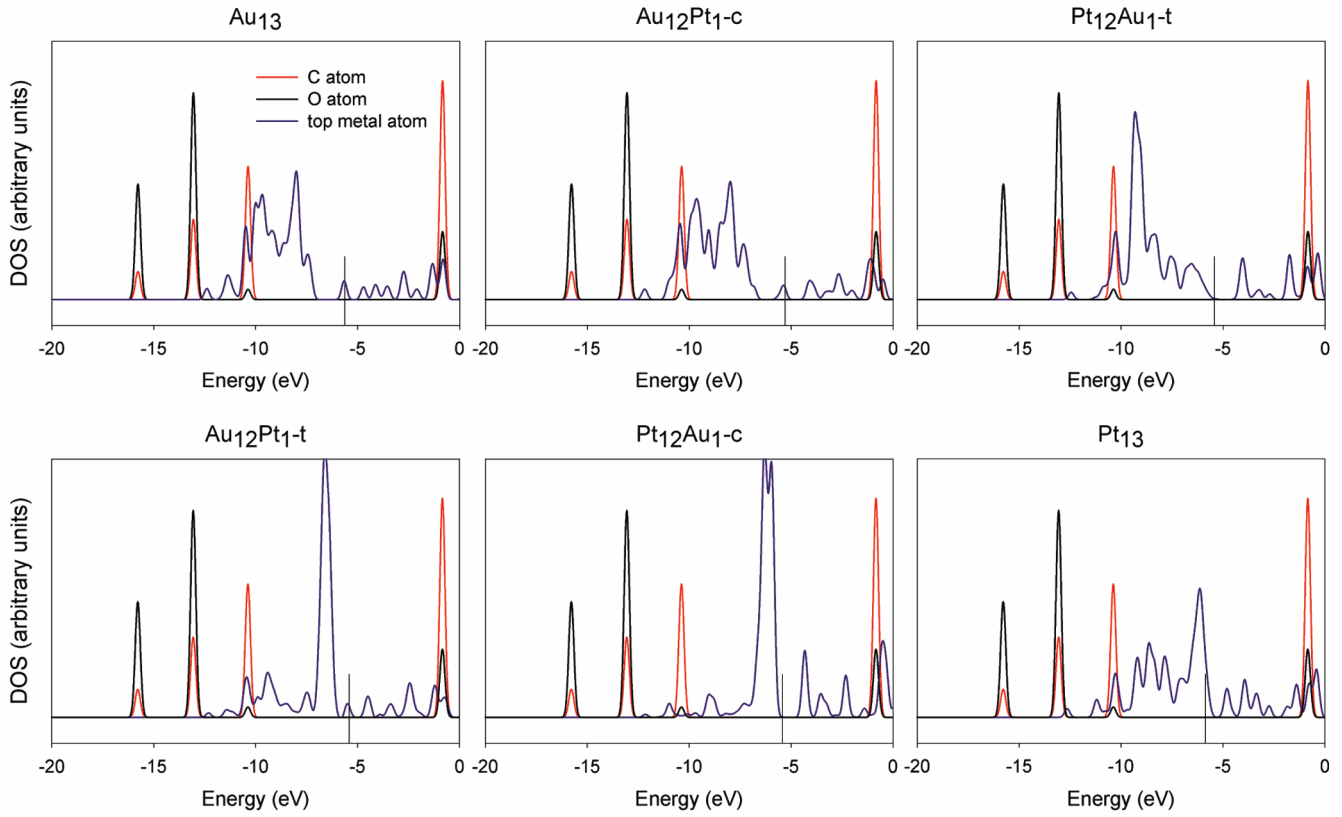

Figure 8. Density of states for the C and O atoms of gas-phase CO (red and black, respectively) and the top atom of the bare metal clusters (blue). The black vertical lines give the Fermi energy for the bare metal clusters.

changes in the metal d-bands can be caused by forming alloys or overlayers or by changing the coordination state of the metal atom.[79,80]

Our results are shown in Figure 8 for the six bare clusters and for CO in vacuum. Here, the energies are all referenced to the vacuum level, and the black vertical lines in each panel indicate the position of the Fermi level in the corresponding bare metal cluster.

In all cases the three CO bands below the clusters' Fermi levels are occupied, while the band located at ∼−1 eV corresponds to the CO LUMO. It is interesting to point out that the cluster composition has a strong effect on the local density of states for both Au (top panels) and Pt (bottom panels) atoms. In particular, we observe a partial occupation of the top energy level in the clusters identified as Au_{13}, $Au_{12}Pt_1$-c, $Au_{12}pt_1$-t, and Pt_{13}, while the top energy level appears fully occupied in the $Pt_{12}Au_1$-t and $Pt_{12}Au_1$-c clusters (a sizable gap exists between HOMO and LUMO for the top metal atom). Furthermore, the cluster composition has a strong effect on the position and intensity of the projection of the d-bands on the top metal atoms. From visual examination of Figure 8, it appears that the d-band is shifted toward higher energies for Pt than for Au. This may have important consequences from a catalysis perspective, based on the importance of the d-band center as discussed above. To quantify this effect, in Figure 9 we plot CO adsorption energy versus the d-band center, calculated as the first moment of the projected d-band density of states on the top atom referenced to the Fermi level.[77] As expected, the d-band center is higher for Pt atoms, which have stronger CO adsorption than Au atoms. In general, CO adsorption is more favorable when the d-band

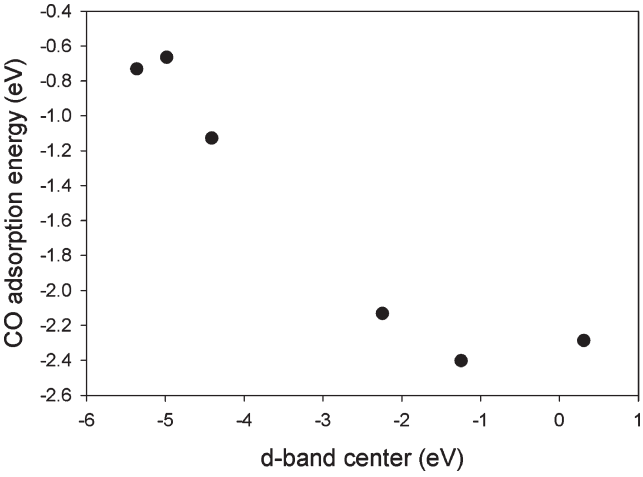

Figure 9. CO adsorption energy as a function of the d-band center of the top metal atom.

center is higher, in qualitative agreement with DFT results obtained using plane-wave approaches on flat surfaces.

The observed differences in the projected DOS become more pronounced upon CO adsorption. In Figure 10 we report the projected DOS on the top metal atom in each cluster, and on C and O atoms of adsorbed CO. The energies are now expressed relative to the Fermi energy of the cluster + CO system. The DOS change significantly compared to those obtained for isolated metal clusters and gas-phase CO. For example, in all cases the metal atoms significantly contribute to the DOS of the

dx.doi.org/10.1021/jp108763f |J. Phys. Chem. C 2011, 115, 5637–5647

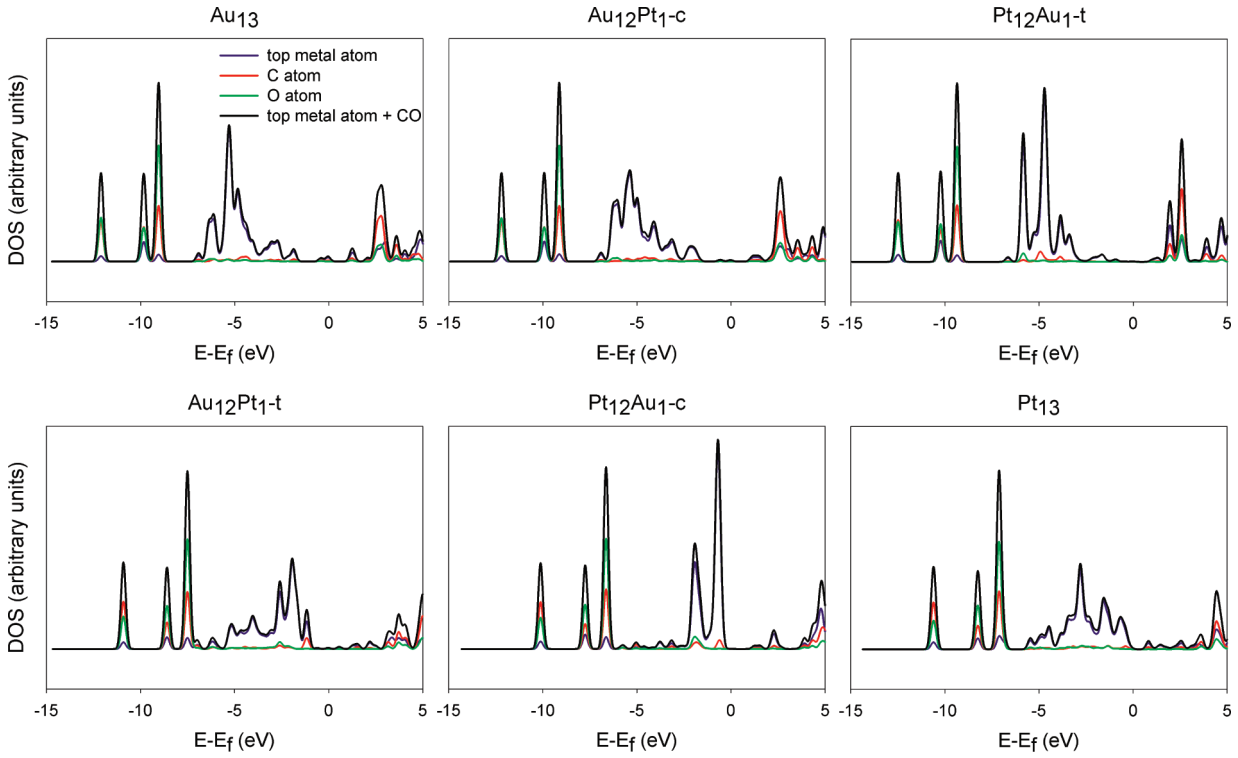

Figure 10. Density of states for the C (red) and O (green) atoms of adsorbed CO and the top atom of the metal clusters with adsorbed CO (blue). The energy is relative to the cluster Fermi energy.

three occupied bands of CO (see the bands at the three lowest energies), a direct consequence of the hybridization upon adsorption.

In all cases, CO adsorption causes large changes in the structure of the d-bands and also in their position with respect to the cluster Fermi energy. This effect is particularly pronounced for Au_{13}, $Pt_{12}Au_1$-t, $Au_{12}Pt_1$-t, and $Pt_{12}Au_1$-c. When CO adsorbs on Au atoms (top panels in Figure 10), the structure of the unoccupied molecular orbitals belonging to both C and O atoms changes significantly compared to that observed for gas-phase CO (in particular, the LUMO observed in gas-phase CO splits in two bands when CO adsorbs). However, very little evidence is provided by the DOS of the top three panels with respect to charge transfer from the metal to CO (only small and rather broad peaks are observed in connection to either C or O atoms at energy levels below the cluster Fermi level but above −8 eV).

When CO adsorbs on Pt atoms (bottom panels in Figure 10), both C and O atoms contribute to a reasonable extent to well-defined occupied orbitals in the range −3 to 0 eV. The effect is less evident on Pt_{13}, on which, however, the charge transfer is still sufficient to change the position of the d-band of the metal atom with respect to that observed before CO adsorption (compare Figure 10 to Figure 8). It is worth pointing out that the metal−C bond (see Table 1) is shorter on $Pt_{12}Au_1$-c than on Pt_{13}, possibly a consequence of the different features of the DOS shown in Figure 10.

To visualize the electronic effects due to CO adsorption and in particular the charge transfer consistent with the back-donation mechanism of Blyholder,[69] in Figure 11 we report plots of the electrostatic potentials of the six cluster + CO systems. In these plots a more negative value (shaded red) indicates higher electron density, while a more positive value (shaded blue) indicates lower electron density. The results indicate that, for CO adsorbed on Au atoms, there is less electron density located around the C and O atoms compared to CO adsorbed on Pt atoms. This difference is consistent with a more significant back-donation of electrons to CO that appears to occur upon adsorption on Pt. The most pronounced back-donation appears on the $Pt_{12}Au_1$-c cluster, for which the metal−C bond is the shortest (see Table 1). Also in qualitative agreement with results for the C−O bond distance (Table 1), the results in Figure 10 suggest that when CO adsorbs on Au (top three panels) the electrostatic potential around the adsorbed CO does not depend significantly on the cluster composition. On the contrary, when CO adsorbs on Pt (bottom three panels in Figure 10), the electrostatic potential shows significant differences depending on the cluster composition.

CONCLUSIONS

We have used DFT calculations to study the adsorption of CO on top of Pt and Au atoms in clusters of 13 atoms. Our results show that the cluster composition affects the adsorption energy and the C−O vibrational frequency even when adsorption occurs on the same metal atom (i.e., Au or Pt). Specifically, when adsorption occurs on Au, increasing the Pt content of the cluster increases the adsorption energy and decreases the C−O vibrational frequency. Increasing the Au content of the cluster when adsorption occurs on Pt yields a decrease in the adsorption energy and an increase in the C−O vibrational frequency.

The electronic structures of the clusters were analyzed to rationalize these observed changes due to the cluster composition. More positive charges on the top Pt atom prior to adsorption result in stronger CO adsorption. For CO adsorption on a given metal, CO + cluster systems with lower HOMO−LUMO gaps have higher adsorption energy. Analysis of the

dx.doi.org/10.1021/jp108763f |J. Phys. Chem. C 2011, 115, 5637–5647

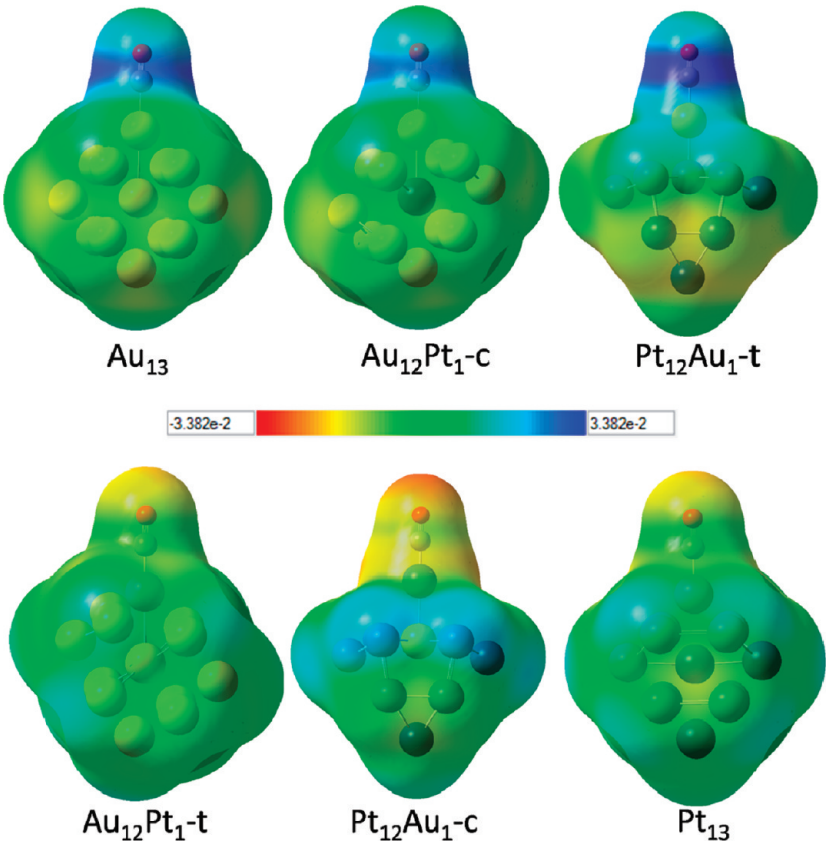

Figure 11. Electrostatic potential of the six clusters with adsorbed CO.

density of states shows the effect of composition on the electronic structure of the clusters, which shifts the d-band and alters the electronic structure of adsorbed CO. Our results suggest that the closer the d-band center is to the Fermi level in the isolated cluster, the more favorable CO adsorption is. The electrostatic potential around the adsorbed CO molecule is more negative, providing evidence for rather significant electronic back-donation, when adsorption occurs on Pt than when CO adsorbs on Au. Collectively, when compared to literature DFT results obtained for CO adsorption on clusters of metal atoms smaller than those considered here, as well as to those obtained for CO adsorption on flat metal surfaces, our results show that the local environment of a transition metal atom determines the properties of adsorbed CO. These effects appear to be strongly dependent on the cluster size, especially for metal clusters of a few atoms.

APPENDIX

The CO adsorption energy calculated using six different exchange-correlation functionals is reported in Figure 12. All six data sets predict adsorption on Pt to be >1 eV more favorable than on Au. In general, the adsorption energies follow the trend described in the main text for B3LYP, with a few exceptions. For example, the adsorption energy on $Au_{12}Pt_1$-t calculated with the PBE1PBE functional is larger than that on $Pt_{12}Au_1$-c and Pt_{13}. The adsorption energy on Pt_{13} calculated with the PBE functional is much lower than that on $Au_{12}Pt_1$-t and $Pt_{12}Au_1$-c. Aside from these differences, which could be due to the geometry minimization procedure for a given structure getting trapped in a local minimum with relatively high energy, the trend discussed in the main text appears to be independent of the choice of exchange-correlation

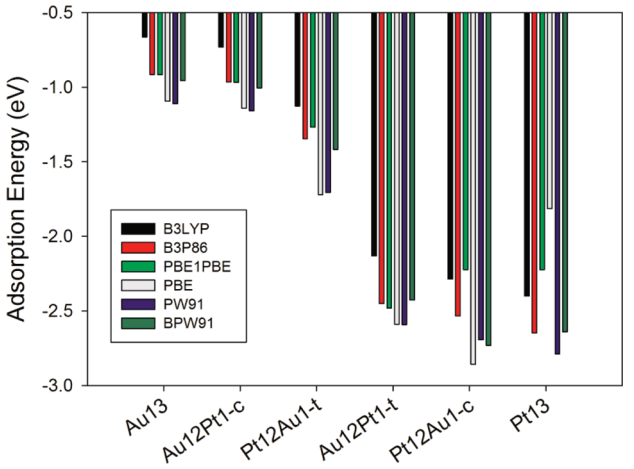

Figure 12. CO adsorption energy on the six clusters for the six functionals considered here.

functional. Calculations using all functionals other than B3LYP predict higher adsorption energies for CO on Au_{13} than the experimental range of 0.54−0.79 eV for CO on Au nanoparticles.[64] Calculations using all functionals except for PBE overestimate the adsorption energy for CO on Pt_{13} compared to the experimental value of −2.13 eV for CO on alumina-supported Pt nanoparticles.[61] Calculations using PBE1PBE and B3LYP come closest to the experimental value, at −2.22 and −2.40 eV, respectively.

In Figure 13 we report the C−O stretching frequency calculated using different functionals. For adsorbed CO, the results follow the trend described in the main text for all of the functionals, with the

dx.doi.org/10.1021/jp108763f |J. Phys. Chem. C 2011, 115, 5637–5647

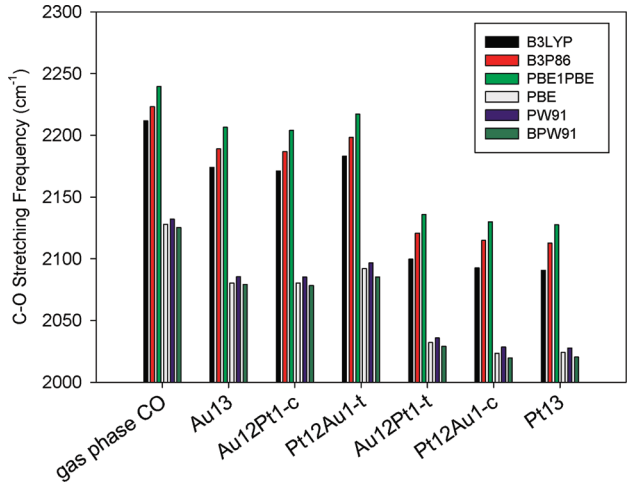

Figure 13. C−O stretching frequency for the six functionals considered here.

highest frequency occurring for CO adsorption on $Pt_{12}Au_1$-t and the lowest frequency occurring for adsorption on Pt_{13}. However, the different functionals produce very different values. Frequencies calculated using hybrid functionals (B3LYP, B3P86, and PBE1PBE) are consistently ∼100 cm^{-1} higher than those calculated using nonhybrid functionals (PBE, PW91, and BPW91). This is because, as previous DFT studies have shown, nonhybrid functionals place occupied energy levels of adsorbates closer to the Fermi level of the metal than hybrid functionals, resulting in more back-donation.[81,82] This results in higher C−O frequencies for hybrid than nonhybrid functionals. Compared to the experimental values[61,68] of ∼2070−2075 cm^{-1} for CO adsorbed on alumina-supported Pt nanoparticles, B3LYP is the most accurate, predicting a frequency ∼15 cm^{-1} higher. B3P86 and PBE1PBE overestimate the frequency by ∼40 and ∼50 cm^{-1}, respectively, while PBE, PW91, and BPW91 all underestimate the frequency by ∼50 cm^{-1}. For CO adsorbed on Au (experimental value[64] of 2123 cm^{-1}), calculations performed using B3LYP, B3P86, and PBE1PBE predict frequencies ∼50, ∼65, and ∼80 cm^{-1} higher, respectively. Calculations performed using PBE, PW91, and BPW91 all predict frequencies ∼40 cm^{-1} lower than the experimental value. Calculations for gas-phase CO follow the same trend, with B3LYP, B3P86, and PBE1PBE giving higher frequencies and PBE, PW91, and BPW91 predicting lower frequencies than the experimental value (2143 cm^{-1}), respectively.

AUTHOR INFORMATION

Corresponding Author

*E mail astriolo@ou.edu; phone 405 325 5716; fax 405 325 5813.

ACKNOWLEDGMENT

The authors acknowledge financial support from the Carbon Nanotube Technology Center (CANTEC) at the University of Oklahoma, funded by the U.S. DOE under contract DE-FG02-06ER64239. M.B.N. has been supported in part by BES, U.S. DOE at ORNL (DE-FG02-98ER14847 and DE-AC05-00OR22725 with UT-Battelle, LLC). Generous allocations of computing time were provided by the OU Supercomputing Center for Education and Research (OSCER) at the University of Oklahoma and by the National Energy Research Scientific Computing Center (NERSC) at Lawrence Berkeley National Laboratory. The authors acknowledge fruitful discussions with Dr. Friederike Jentoft and Dr. Richard Mallinson of the University of Oklahoma.

REFERENCES

(1) Ferrando, R.; Jellinek, J.; Johnston, R. L. *Chem. Rev.* **2008**, *108* (3), 845–910.
(2) Dimitratos, N.; Messi, C.; Porta, F.; Prati, L.; Villa, A. *J. Mol. Catal A: Chem.* **2006**, *256* (1−2), 21–28.
(3) Selvarani, G.; Selvaganesh, S. V.; Krishnamurthy, S.; Kiruthika, G. V. M.; Sridhar, P.; Pitchumani, S.; Shukla, A. K. *J. Phys. Chem. C* **2009**, *113* (17), 7461–7468.
(4) Comotti, M.; Pina, C. D.; Rossi, M. *J. Mol. Catal A: Chem.* **2006**, *251* (1−2), 89–92.
(5) Petkov, V.; Shastri, S. D. *Phys. Rev. B* **2010**, *81* (16), 165428.
(6) Sankaranarayanan, S. K. R. S.; Bhethanabotla, V. R.; Joseph, B. *Phys. Rev. B* **2005**, *72*, 195405.
(7) Huang, S.-P.; Mainardi, D. S.; Balbuena, P. B. *Surf. Sci.* **2003**, *545*, 163–179.
(8) Calvo, S. R.; Balbuena, P. B. *Surf. Sci.* **2005**, *581* (2−3), 213–224.
(9) Morrow, B. H.; Striolo, A. *Phys. Rev. B* **2010**, *81* (15), 155437.
(10) Pestryakov, A. N.; Bogdanchikova, N.; Simakov, A.; Tuzovskaya, I.; Jentoft, F.; Farias, M.; Díaz, A. *Surf. Sci.* **2007**, *601* (18), 3792–3795.
(11) Bell, A. T. *Science* **2003**, *299* (5613), 1688–1691.
(12) Carrette, L.; Friedrich, K. A.; Stimming, U. *ChemPhysChem* **2000**, *1* (4), 162–193.
(13) Khodakov, A. Y.; Chu, W.; Fongarland, P. *Chem. Rev.* **2007**, *107* (5), 1692–1744.
(14) Desai, S.; Neurock, M. *Electrochim. Acta* **2003**, *48* (25−26), 3759–3773.
(15) Zhang, C.; Hu, P.; Alavi, A. *J. Am. Chem. Soc.* **1999**, *121* (34), 7931–7932.
(16) Ford, D. C.; Xu, Y.; Mavrikakis, M. *Surf. Sci.* **2005**, *587* (3), 159–174.
(17) Doll, K. *Surf. Sci.* **2004**, *573* (3), 464–473.
(18) Alayoglu, S.; Nilekar, A. U.; Mavrikakis, M.; Eichhorn, B. *Nat. Mater.* **2008**, *7* (4), 333–338.
(19) Nilekar, A. U.; Alayoglu, S.; Eichhorn, B.; Mavrikakis, M. *J. Am. Chem. Soc.* **2010**, *132* (21), 7418–7428.
(20) Yudanov, I. V.; Sahnoun, R.; Neyman, K. M.; Rosch, N.; Hoffmann, J.; Schauermann, S.; Johanek, V.; Unterhalt, H.; Rupprechter, G.; Libuda, J.; Freund, H.-T. *J. Phys. Chem. B* **2003**, *107* (1), 255–264.
(21) Sadek, M. M.; Wang, L. *J. Phys. Chem. A* **2006**, *110* (51), 14036–14042.
(22) Song, S.; Ge, Q.; Wang, L. *J. Phys. Chem. B* **2005**, *109* (47), 22341–22350.
(23) Pedersen, M. Ø.; Helveg, S.; Ruban, A.; Stensgaard, I.; Lægsgaard, E.; Nørskov, J. K.; Besenbacher, F. *Surf. Sci.* **1999**, *426* (3), 395–409.
(24) Habrioux, A.; Vogel, W.; Guinel, M.; Guetaz, L.; Servat, K.; Kokoh, B.; Alonso-Vante, N. *Phys. Chem. Chem. Phys.* **2009**, *11* (18), 3573–3579.
(25) Irissou, E.; Laplante, F.; Garbarino, S.; Chaker, M.; Guay, D. *J. Phys. Chem. C* **2010**, *114* (5), 2192–2199.
(26) Vajda, S.; Pellin, M. J.; Greeley, J. P.; Marshall, C. L.; Curtiss, L. A.; Ballentine, G. A.; Elam, J. W.; Catillon-Mucherie, S.; Redfern, P. C.; Mehmood, F.; Zapol, P. *Nat. Mater.* **2009**, *8* (3), 213–216.
(27) Xiao, L.; Wang, L. *J. Phys. Chem. A* **2004**, *108* (41), 8605–8614.
(28) Morrow, B. H.; Striolo, A. *J. Phys. Chem. C* **2007**, *111* (48), 17905–17913.
(29) Morrow, B. H.; Striolo, A. *Nanotechnology* **2008**, *19* (19), 195711.
(30) Morrow, B. H.; Striolo, A. *Mol. Simul.* **2009**, *35* (10/11), 795–803.
(31) Frisch, M. J.; Trucks, G. W.; Schlegel, H. B.; Scuseria, G. E.; Robb, M. A.; Cheeseman, J. R.; Montgomery, J. J. A.; Vreven, T.; Kudin,

K. N.; Burant, J. C.; Millam, J. M.; Iyengar, S. S.; Tomasi, J.; Barone, V.; Mennucci, B.; Cossi, M.; Scalmani, G.; Rega, N.; Petersson, G. A.; Nakatsuji, H.; Hada, M.; Ehara, M.; Toyota, K.; Fukuda, R.; Hasegawa, J.; Ishida, M.; Nakajima, T.; Honda, Y.; Kitao, O.; Nakai, H.; Klene, M.; Li, X.; Knox, J. E.; Hratchian, H. P.; Cross, J. B.; Bakken, V.; Adamo, C.; Jaramillo, J.; Gomperts, R.; Stratmann, R. E.; Yazyev, O.; Austin, A. J.; Cammi, R.; Pomelli, C.; Ochterski, J. W.; Ayala, P. Y.; Morokuma, K.; Voth, G. A.; Salvador, P.; Dannenberg, J. J.; Zakrzewski, V. G.; Dapprich, S.; Daniels, A. D.; Strain, M. C.; Farkas, O.; Malick, D. K.; Rabuck, A. D.; Raghavachari, K.; Foresman, J. B.; Ortiz, J. V.; Cui, Q.; Baboul, A. G.; Clifford, S.; Cioslowski, J.; Stefanov, B. B.; Liu, G.; Liashenko, A.; Piskorz, P.; Komaromi, I.; Martin, R. L.; Fox, D. J.; Keith, T.; Al-Laham, M. A.; Peng, C. Y.; Nanayakkara, A.; Challacombe, M.; Gill, P. M. W.; Johnson, B.; Chen, W.; Wong, M. W.; Gonzalez, C.; Pople, J. A. *Gaussian 03*, revision E.01; Gaussian, Inc.: Wallingford, CT, 2004.

(32) Becke, A. D. *J. Chem. Phys.* **1993**, *98* (7), 5648–5652.

(33) Lee, C.; Yang, W.; Parr, R. G. *Phys. Rev. B* **1988**, *37*, 785.

(34) Vosko, S. H.; Wilk, L.; Nusair, M. *Can. J. Phys.* **1980**, *58* (8), 1200–1211.

(35) Stephens, P. J.; Devlin, F. J.; Chabalowski, C. F.; Frisch, M. J. *J. Phys. Chem.* **1994**, *98* (45), 11623–11627.

(36) Perdew, J. P. *Phys. Rev. B* **1986**, *33* (12), 8822.

(37) Becke, A. D. *Phys. Rev. A* **1988**, *38* (6), 3098.

(38) Perdew, J. P. In *Electronic Structure of Solids '91*; Ziesche, P., Eschrig, H., Eds.; Akademie Verlag: Berlin, Germany, 1991; p 11.

(39) Perdew, J. P.; Chevary, J. A.; Vosko, S. H.; Jackson, K. A.; Pederson, M. R.; Singh, D. J.; Fiolhais, C. *Phys. Rev. B* **1992**, *46* (11), 6671.

(40) Perdew, J. P.; Burke, K.; Ernzerhof, M. *Phys. Rev. Lett.* **1996**, *77* (18), 3865.

(41) Adamo, C.; Barone, V. *J. Chem. Phys.* **1999**, *110* (13), 6158–6170.

(42) Giuffrida, S.; Barone, G.; Duca, D. *J. Chem. Inf. Model.* **2009**, *49* (5), 1223–1233.

(43) de Souza Monteiro, R.; Paes, L.; de, M.; Carneiro, J.; Aranda, D. *J. Cluster Sci.* **2008**, *19* (4), 601–614.

(44) Zeinalipour-Yazdi, C. D.; Cooksy, A. L.; Efstathiou, A. M. *Surf. Sci.* **2008**, *602* (10), 1858–1862.

(45) Shimodaira, Y.; Tanaka, T.; Miura, T.; Kudo, A.; Kobayashi, H. *J. Phys. Chem. C* **2007**, *111* (1), 272–279.

(46) Hay, P. J.; Wadt, W. R. *J. Chem. Phys.* **1985**, *82* (1), 299–310.

(47) *CRC Handbook of Chemistry and Physics*, 81st ed; Lide, D. R., Ed.; CRC Press: Boca Raton, FL, 2000.

(48) O'Boyle, N. M.; Tenderholt, A. L.; Langner, K. M. *J. Comput. Chem.* **2008**, *29* (5), 839–845.

(49) Carpenter, J. E.; Weinhold, F. *J. Mol. Struct. THEOCHEM* **1988**, *169*, 41–62.

(50) Foster, J. P.; Weinhold, F. *J. Am. Chem. Soc.* **1980**, *102* (24), 7211–7218.

(51) Liu, H. B.; Pal, U.; Ascencio, J. A. *J. Phys. Chem. C* **2008**, *112* (49), 19173–19177.

(52) Xiao, S.; Hu, W.; Luo, W.; Wu, Y.; Li, X.; Deng, H. *Eur. Phys. J. B* **2006**, *54* (4), 479–484.

(53) Yang, Z.; Yang, X.; Xu, Z.; Liu, S. *Phys. Chem. Chem. Phys.* **2009**, *11* (29), 6249–6255.

(54) Reyes-Nava, J. A.; Rodriguez-Lopez, J. L.; Pal, U. *Phys. Rev. B* **2009**, *80*, 161412.

(55) Henglein, A. *J. Phys. Chem. B* **2000**, *104* (10), 2201–2203.

(56) Hodak, J. H.; Henglein, A.; Hartland, G. V. *J. Chem. Phys.* **2001**, *114* (6), 2760–2765.

(57) Garcia-Gutierrez, D. I.; Gutierrez-Wing, C. E.; Giovanetti, L.; Ramallo-Lopez, J. M.; Requejo, F. G.; Jose-Yacaman, M. *J. Phys. Chem. B* **2005**, *109* (9), 3813–3821.

(58) Yang, J.; Yang Lee, J.; Too, H.-P. *Plasmonics* **2006**, *1* (1), 67–78.

(59) Wang, S.; Kristian, N.; Jiang, S.; Wang, X. *Nanotechnology* **2009**, *20* (2), 025605.

(60) Zhang, W.; Li, L.; Du, Y.; Wang, X.; Yang, P. *Catal. Lett.* **2009**, *127* (3), 429–436.

(61) Bourane, A.; Dulaurent, O.; Bianchi, D. *J. Catal.* **2000**, *196* (1), 115–125.

(62) Yeo, Y. Y.; Vattuone, L.; King, D. A. *J. Chem. Phys.* **1997**, *106* (1), 392–401.

(63) Huang, Y.-W.; Lee, S.-L. *Chem. Phys. Lett.* **2010**, *492* (1−3), 98–102.

(64) Meier, D. C.; Goodman, D. W. *J. Am. Chem. Soc.* **2004**, *126* (6), 1892–1899.

(65) Yim, W.-L.; Nowitzki, T.; Necke, M.; Schnars, H.; Nickut, P.; Biener, J.; Biener, M. M.; Zielasek, V.; Al-Shamery, K.; Klüner, T.; Bäumer, M. *J. Phys. Chem. C* **2006**, *111* (1), 445–451.

(66) Chen, L.; Chen, B.; Zhou, C.; Wu, J.; Forrey, R. C.; Cheng, H. *J. Phys. Chem. C* **2008**, *112*, 13937–13942.

(67) Ren, H.; Humbert, M. P.; Menning, C. A.; Chen, J. G.; Shu, Y.; Singh, U. G.; Cheng, W.-C. *Appl. Catal., A* **2010**, *375* (2), 303–309.

(68) Gruene, P.; Fielicke, A.; Meijer, G.; Rayner, D. M. *Phys. Chem. Chem. Phys.* **2008**, *10* (40), 6144–6149.

(69) Blyholder, G. *J. Phys. Chem.* **1964**, *68* (10), 2772–2777.

(70) Babarao, R.; Jiang, J.; Sandler, S. I. *Langmuir* **2008**, *25* (9), 5239–5247.

(71) Mulliken, R. S. *J. Chem. Phys.* **1955**, *23* (10), 1833–1840.

(72) Besler, B. H.; M., K. M., Jr.; Kollman, P. A. *J. Comput. Chem.* **1990**, *11* (4), 431–439.

(73) Reed, A. E.; Curtiss, L. A.; Weinhold, F. *Chem. Rev.* **1988**, *88* (6), 899–926.

(74) Zhou, Z.; Parr, R. G. *J. Am. Chem. Soc.* **1990**, *112* (15), 5720–5724.

(75) Aihara, J.-i. *Phys. Chem. Chem. Phys.* **2000**, *2* (14), 3121–3125.

(76) Ruban, A.; Hammer, B.; Stoltze, P.; Skriver, H. L.; Nørskov, J. K. *J. Mol. Catal A: Chem.* **1997**, *115* (3), 421–429.

(77) Kitchin, J. R.; Norskov, J. K.; Barteau, M. A.; Chen, J. G. *J. Chem. Phys.* **2004**, *120* (21), 10240–10246.

(78) Mavrikakis, M.; Hammer, B.; Norskov, J. K. *Phys. Rev. Lett.* **1998**, *81* (13), 2819.

(79) Hammer, B.; Nielsen, O. H.; Norskov, J. K. *Catal. Lett.* **1997**, *46* (1), 31–35.

(80) Hammer, B.; Norskov, J. K. *Phys. Rev. Lett.* **1997**, *79* (22), 4441.

(81) Neef, M.; Doll, K. *Surf. Sci.* **2006**, *600* (5), 1085–1092.

(82) Gil, A.; Clotet, A.; Ricart, J. M.; Kresse, G.; García-Hernández, M.; Rösch, N.; Sautet, P. *Surf. Sci.* **2003**, *530* (1−2), 71–87.